Characterization and Inhibition of SARS-Coronavirus Main Protease

Po-Huang Liang*

Institute of Biological Chemistry, Academia Sinica, Taipei 11529, Taiwan R.O.C

Abstract: Severe acute respiratory syndrome (SARS) is an emerging infectious disease caused by a novel human coronavirus (CoV). During the 2003 epidemic, the disease rapidly spread from its origin in southern China to other countries and affected almost 8000 patients, which resulted in about 800 fatalities. A chymotrypsin-like cysteine protease named 3C-like protease ($3CL^{pro}$) is essential for the life cycle of the SARS-CoV. This main protease is responsible for maturation of functional proteins and represents a key anti-viral target. HPLC and fluorescence-based assays have been used to characterize the protease and to determine the potency of the inhibitors. The fluorogenic method monitoring the increase of fluorescence from the cleavage of a peptide substrate containing an Edans-Dabcyl fluorescence quenching pair at two ends has enabled the use of high throughput screening to speed up the drug discovery process. Several groups of inhibitors have been identified through high throughput screening and rational drug design approaches. Thus, α,β-unsaturated peptidomimetics, anilides, metal-conjugated compounds, boronic acids, quinolinecarboxylate derivatives, thiophenecarboxylates, phthalhydrazide-substituted ketoglutamine analogues, isatin and natural products have been identified as potent inhibitors of the SARS-CoV main protease. The different classes of inhibitors reported in these studies are summarized in this review. Some of these inhibitors could be developed into potential drug candidates, which may provide a solution to combat possible reoccurrence of the SARS and other life-threatening viruses with 3CL proteases.

Keywords: SARS coronavirus, cysteine protease, fluorescence assay, high throughput screening, rational drug design, inhibitor.

GENERAL INTRODUCTION

Severe acute respiratory syndrome (SARS) is an atypical pneumonial infection featured by non-productive cough, high fever and headache that may progress to generalized interstitial infiltrates in the lung. This recently emerging disease first occurred in the Guangdon province of China in late 2002 and subsequently spread to over 25 countries in 2003. SARS is caused by a novel human coronavirus (CoV) named SARS-CoV [1–6]. This virus belongs to the coronaviridae family (see Fig. (**1**) for sequence homology of their main proteases), which includes porcine transmissible gastroenteritis virus (TGEV), human coronavirus (HCoV) 229E, mouse hepatitis virus (MHV), bovine coronavirus (BCoV), and porcine epidemic diarrhea virus (PEDV) (7–9). These coronaviruses are large, enveloped, positive single-stranded RNA viruses containing 27–31 kb genomes, which cause respiratory and enteric diseases in humans and other animals. The SARS-CoV genome comprises of about 29,700 nucleotides which encode non-structural proteins and structural proteins. Two overlapping replicase polyproteins, pp1a (486 kDa) and pp1ab (790 kDa), mediate all the functions required for viral replication and transcription [10,11]. These non-structural polyproteins are autocatalytically processed through the virally encoded main protease and papain-like protease to yield mature proteins including the RNA-dependent RNA polymerase (RdRp), the RNA helicase, and other proteins whose functions are not well characterized [12] (Fig. (**2**)). The main protease is called 3C-like protease ($3CL^{pro}$) since it is analogous to the 3C proteases encoded by picornaviruses [13]. Due to its pivotal role in the SARS-CoV life cycle, the $3CL^{pro}$ has been considered to be a promising target for anti-SARS drug discovery.

Other than the non-structural proteins, the structural proteins of coronaviruses including S (spike), E (envelope), M (membrane), and N (nucleocapsid) proteins function during host cell entry and virion morphogenesis and release [14]. S protein on the surface of the virus is a membrane glycoprotein responsible for virus attachment to the host receptor which was identified to be angiotensin converting enzyme II on human cells for SARS-CoV [15]. N binds to a defined packing signal on viral RNA, leading to the formation of the helical nucleocapsis. M is localized at intracellular membrane structures and interact with nucelocapsid to form a viral core structure. The conserved segments of the S, E, M, and N proteins can be found in SARS-CoV and related coronaviruses [2]. These proteins including N, E, M, and truncated forms of the S (S1-S7) of SARS-CoV have been expressed in *Escherichia coli* and six proteins N, E, M, S2, S5, and S6 were used for Western blot to detect various immunoglobulin classes in serum samples from probable SARS patients [16]. The results indicated that N was recognized in most of the sera. In some cases, S6 could be recognized as early as 2 or 3 days after illness onset, while S5 was recognized at a later stage.

SARS-CoV $3CL^{pro}$ cleaves pp1a at the predicted 11 conserved sites with a conserved sequence of (Leu,Met,Phe)-GlnØ(Ser,Ala,Gly), in which a P1 glutamine residue invariably occupies the S1 subsite [17] (see the bottom panel in Fig. (**2**)). The protease is a chymotypsin-like protease but uses a Cys rather than a Ser residue as the active site nucleophile [18]. Moreover, the active site of the SARS

*Address correspondence to this author at the Institute of Biological Chemistry, Academia Sinica, Taipei 11529, Taiwan R.O.C.; Tel: 886-2-2785-5696; Ext: 6070; Fax: 886-2-2788-9759; E-mail: phliang@gate.sinica.edu.tw

1568-0266/06 $50.00+.00

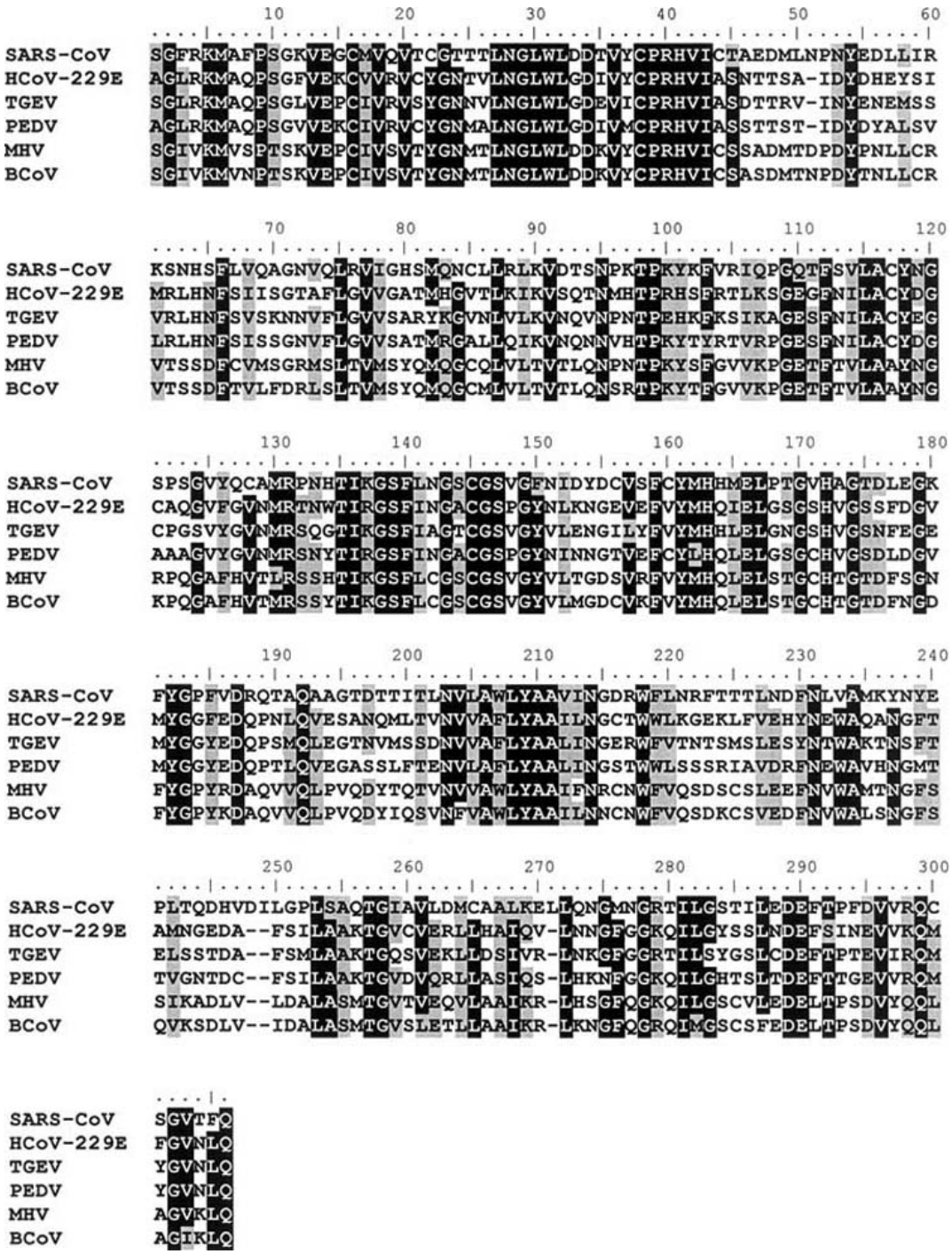

Fig. (1). Sequence homology of the 3CL^{pro} from a group of coronaviruses including SARS-CoV, HCoV 229E, TGEV, PEDV, MHV, and BCoV. The numbering is according to that for SARS 3CL^{pro}. Catalytic dyad C145 and His41 are totally conserved in all the sequences.

protease comprises a catalytic dyad Cys145 and His41 rather than a triad [18,19]. The protease contains three domains and the active site is located between domain I and II. Several crystal structures of coronavirus 3CL^{pro} (apo form or with suicide inhibitors) reported from TGEV, HCoV 229E and SARS-CoV (18, 20–22) reveal a common feature in 3CL^{pro}: two chymotrypsin-like β-domains (residues 1–184) and one α-helical dimerization domain (residues 201–303). The additional helical C-terminal domain of about 100 residues, absent from the analogous picornavirus 3C protease and chymotrypsin, is essential for dimerization of the 3CL^{pro} and its enzymatic activity [20,23]. In addition to the C-terminus, the N-finger containing a number of N-terminal amino acids is important for enzyme activity of the main proteases from TEGV and SARS-CoV since the deletion of the N-finger abolishes enzyme activity [20,24].

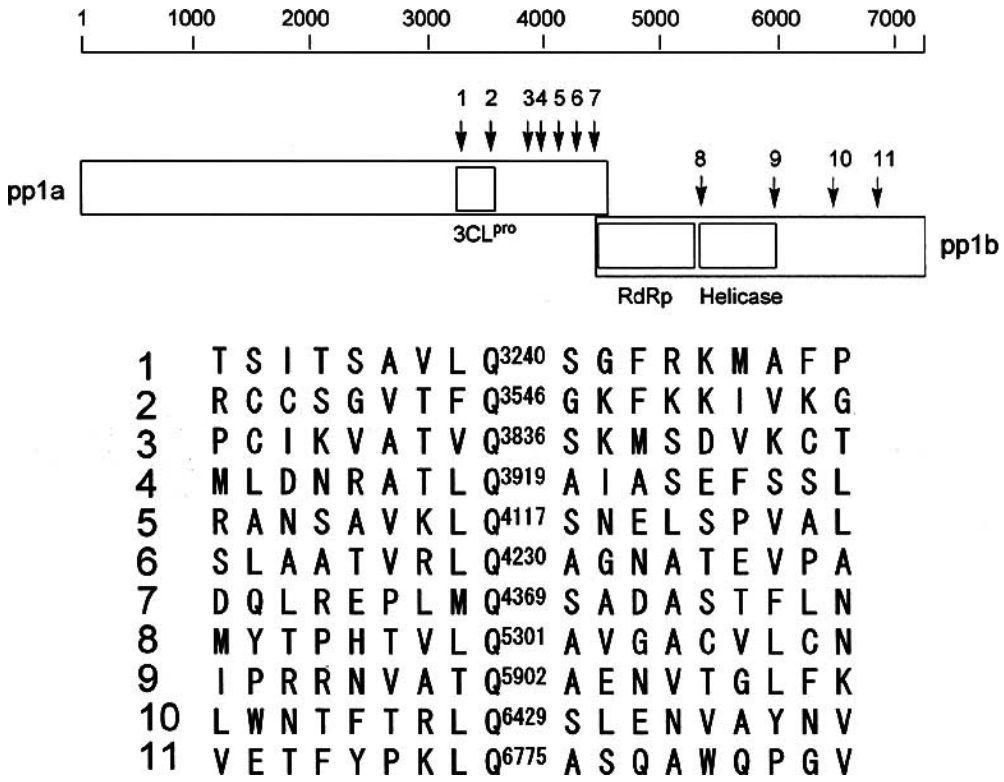

Fig. (2). The two SARS-CoV polyproteins, pp1a and pp1ab (pp1a + pp1b), with $3CL^{pro}$ cleavage sites indicated in arrows. The amino acid numbering of the polyproteins is marked at the top. The eleven cleavage sites with conserved amino acid sequences are shown in the bottom panel. The proteolytic processing at different sites could result in maturation of nsp (non-structural proteins). Some predicted end-products of the cleavage including $3CL^{pro}$ itself, RdRp (RNA-dependent RNA polymerase) and helicase are shown.

HPLC and fluorescence-based methods have been used to characterize the protease kinetics and inhibition. The HPLC method is used to monitor the formation of product peaks from the substrate peak [17]. A fluorogenic substrate is used in the fluorescence assay and the increase of fluorescence from the cleavage of a substrate that contains fluorescence quenching pair at the N- and C-termini is measured [25]. The latter method is fast, can be automated, and is thus suitable for high throughput assay. Many inhibitors have been discovered through high throughput random screening and rational design by using either the HPLC or the fluorescence-based assay (*vide infra*).

In this review, the assay methods, the dimerization of the SARS-CoV $3CL^{pro}$, the 3-D structures of the protease, and the inhibitors identified so far are summarized and discussed. There is currently no effective treatment for the SARS disease. A combination of Ribavirin for antivirus and corticosteroids for immunomodulation has been used to treat SARS patients [26–30]. However, Ribavirin at non-toxic concentration has little *in-vitro* inhibitory activity against SARS-CoV [31]. Improved clinical outcome has been reported for patients receiving early administration with the HIV drug Kaletra plus Ribavirin, and the corticosteroids [32] or Lopinavir/Ritonavir [33]. Human interferons were also reported to be effective against SARS [31,34], but there is no clear evidence to support the clinical observation. The data summarized here serve as a firm basis for therapeutic method development to deal with the possible reoccurrence of SARS in the future and may also lead to new drugs for other viral diseases caused by the viruses with similar proteases.

ASSAY OF THE PROTEASE ACTIVITY

The recombinant SARS main protease has been initially expressed and purified by different laboratories [17,25,35, 36]. Some recombinant forms of the protease contained C-terminal Hexa-His tag used for Ni-NTA column chromatography or N-terminal extra amino acids left from incomplete tag removal using thrombin cleavage [17,35,36]. Some laboratories used FXa with its cleavage site engineered in the N-terminus of the protease to remove the affinity tag and yielded recombinant protease with authentic amino acid sequence [25]. These recombinant proteins have different properties especially in dimerization as described below.

A HPLC method was first used to assay the activity of the protease. Products generated from a peptide substrate such as H_2N-TSAVLQØSGFRKW-COOH (the cleavage site is indicated with ↓) can be separated by using a reverse-phase HPLC column and a linear gradient of acetonitrile [17]. The absorbance can be measured at 215 or 280 nm and the peak areas can be integrated to calculate the rate of protease reaction. The kinetic parameters were determined by fitting the data with the Michaelis-Menten equation. The 11 peptides corresponding to the possible cleavage sites (Fig. (**2**)) of the SARS main protease on the pp1a and pp1ab polyproteins were tested as substrates for the protease and the peptides spanning the protease's own N- and C-termini

were the best substrates [17]. The conserved core sequence of the native cleavage sites of the protease was confirmed to be optimal for high hydrolytic activity in a more detailed study using 34 synthetic peptides as substrates [37]. Amino acids at position P3, P4 and P3' were found to be critical for substrate recognition. Increasing the β-sheet character of the substrates was also important.

However, for high throughput screening to identify inhibitors, a more convenient assay method was required. Our laboratory has utilized a fluorogenic substrate (Dabcyl-KTSAVLQSGFRKME-Edans) which can be cleaved by the protease resulting in an intense increase in fluorescence [25,38]. The two fluorescent groups Dabcyl and Edans form a quenching pair and the fluorescence of Edans is reduced by Dabcyl, which is at a proximal short distance (in this case 14 amino acids away), but the fluorescence becomes high when the peptide is cleaved by the protease. This fluorescence resonance energy transfer (FRET) technology has been demonstrated to be useful for assaying retroviral proteases [39]. The fluorescence-based assay has become the method of choice to evaluate the potencies of inhibitors from high throughput screening. Some of the fluorogenic substrates used for the assay include Dabcyl-Leu-Ala-Gln-Ala-Val-Arg-Ser-Ser-Ser-Arg-Edans [35], Abz-Ser-Val-Thr-Leu-Gln-Ser-Gly-Tyr(NO_2)-Arg [40], and Abz-DNP quenching pair [41].

DIMERIZATION OF THE PROTEASE

There is a number of reports in the literature which show that a protease can exist as a monomer or a dimer and only the dimer is active [42–44]. Size exclusion, the measurements of activity versus enzyme concentration, and analytic ultracentrifugation (AUC) are examples of tools that have been used to measure the monomer-dimer equilibria. However, there is controversy on the reported dissociation constants of the dimeric SARS main protease. As mentioned above, different recombinant forms of the SARS $3CL^{pro}$ containing no or extra amino acids at either the N- or C-terminus have been used for these studies. The properties of these recombinant proteases are somewhat different. This discrepancy seems to result from the different monomer-dimer equilibria probably due to the interference of those extra amino acids in dimer formation, different pH, different protein concentration, and/or the tools of measurement used. A K_d of 100 μM was determined by Fan *et al.* for the recombinant SARS protease containing a C-terminal His_6 using the gel filtration size exclusion method [17]. The enzyme existed as a mixture of monomer and dimer at a higher protein concentration (4 mg/mL ~118 μM) and exclusively as a monomer at a lower protein concentration (0.2 mg/mL ~6 μM), as revealed by analytical gel filtration. The dissociation constant K_d of the dimer was thus estimated to be 100 μM. The recombinant proteins prepared by Bacha *et al.* contained extra amino acids at the N-terminus and their enzyme existed largely in the monomeric forms, similar to that observed by Fan *et al.* [35].

Using the fluorescence assay, we determined the K_d of the protease which had authentic amino acid sequence (i.e., without extra amino acid residues) [25]. An enzyme concentration range of 5–150 nM or 50–3000 nM with 60 μM fluorogenic substrate were used to determine the K_d. The plot fitting of reaction rate versus enzyme concentration becomes non-linear when the enzyme concentration approaches the dimer K_d, verifying the monomer is inactive, and the apparent K_d value for the dimer-monomer equilibrium of our enzyme was measured to be 15 nM. Thus, this K_d (15 nM) is remarkably smaller than the one (100 μM) previously estimated from the analytical gel filtration experiments.

We also performed size exclusion chromatography and at both high (4 mg/mL) and low (0.2 mg/mL) enzyme concentrations, and the SARS main protease showed a predominant peak of the dimer. Analytical ultracentrifugation (AUC) method was utilized to examine the quaternary structures of the wild-type $3CL^{pro}$ and the C145A mutant protease (to prevent autoactivation) containing additional N- or C-terminal segments of the polyprotein sequences to compare the K_d values of their dimers [22]. The AUC data for the wild-type SARS protease indicate that the determined molecular weight is that of a dimer and the dimeric wild-type protein has a K_d of 0.35 nM. In contrast, the recombinant protease, which contains 10 extra amino acids belonging to its own self-cleavage site at the N- or C-terminus, shows 49- and 16-fold larger K_d values (17.2 nM and 5.6 nM), respectively. Therefore, even with only 10 extra amino acids in the N- or C-terminus, dimer formation was impeded. However, the sub-μM K_d value of the protease indicates that immature $3CL^{pro}$ can form a small amount of dimer enabling it to undergo autoprocessing to yield the mature protein, which further serves as a seed for facilitated maturation [22]. From the above studies, the extra amino acids at the N- and/or C-terminus of the protease apparently affect the dimer formation.

However, using the AUC method, Chou *et al.* reported a K_d of 190 nM at pH 8, even though the recombinant protease contained a His_6-tag at its C-terminus [45]. On the other hand, deletion of N-terminal amino acids increased the K_d and decreased the protease activity, suggesting that the N-finger is important for dimer formation. The sequential deletion of the first 3 and 7 residues at the N-terminus caused a 12- and 1275-fold increase in dimer K_d, respectively [24]. Particularly, the Arg4 is the most important one for dimer formation since deletion of the first 3 residues caused only a 12-fold increase in K_d, whereas deletion of the first 4 residues caused a 205-fold increase in K_d. From the crystal structure, the N-terminal residues 1–7 (N-finger) is buried in the dimer interface with numerous contacts with the domain II close to the active site of the other protomer [21,22]. In conclusion, the extra exogenous amino acids and the lack of the first 4 residues at the N-terminus cause a greater impact on protease dimerization.

3-D STRUCTURES OF THE PROTEASE

The first crystal structure of SARS-CoV main protease and its complex with a substrate-like hexapeptidyl chloromethylketone (CMK) inhibitor were reported by Rao and his coworkers [21]. Analogous to the previously solved structure of coronavirus main protease from TGEV [18], the SARS protease forms a dimer with two protomers oriented almost at right angle to each other. Each protomer is composed of three domains, which include the N-terminal domain I (residues 8–101) and the domain II (residues

102–184) having an antiparallel β-barrel structure. In contrast, the C-terminal domain III (residues 201–303) contains five α-helices arranged into a large antiparallel globular cluster, and is connected with domain II through a loop region (residues 185–200). The Cys-His catalytic dyad is located in an active site cleft between domains I and II.

A. pH Variation of Structures

At pH 6.0, an analysis of the crystal structure of the SARS protease indicates that the protomer A has a structure similar to those of the other coronavirus main proteases at pH 7.6 (active form), but the protomer B shows the collapsed active site due to the lower pH (inactive form). The pH profile of the enzyme activity confirmed that the protease is fully active at pH above 7, but the activity is dramatically decreased at pH 6. As shown in protomer A, the oxyanion hole and the N-finger of protomer B docks to its binding site, the main-chain NH of Gly143(A) is available for H-bonding to the oxyanion intermediate and the side-chain NH_2 of His163(A) imidazole ring is free to bind with P1 Gln of the substrate. In the inactive conformation of protomer B, these interactions are absent and the N-finger of protomer A is not docked to its binding site. This results in the collapse of the oxyanion hole with protrusion of F140(B) into the bulk solvent and conformational switching of Glu166(B), thereby blocking the substrate site.

B. Substrate-Binding Subsites

The S1 subsite in protomer A (active form) consists of the side chains of His163(A) and Phe140(A) as well as the main chains of Met165(A), Glu166(A) and His172(A). Glu166(A) side chain forms a salt bridge with His172(A) and also interacts with the amide group of the N-terminal Ser1 from protomer B. The N-finger (Residues 1–7) plays an important role in the dimerization and formation of the active site. With the hexapeptidyl CMK (Cbz-Val-Asn-Ser-Thr-Leu-Gln-CMK) inhibitor bound, a covalent bond is formed between the Sγ atom of Cys145 and the methylene group of the CMK. The structure of the complex at 2.5 Å resolution reveals an unexpected mode of inhibitor binding [21]. In the protomer A (the active form), the side-chain carbonyl of P1-Gln accepts a H-bond (2.8 Å) from the Nε2 atom of His163(A). The side chain Nε2 of P1-Gln donates a H-bond to the side chain carbonyl of the conserved Glu166(A). However, P2-Leu fails to bind to the S2 subsite in the vincity of Asp 187 and becomes solvent exposed. This noncanonical binding results in a frameshift in the subsite interaction: P3-Thr and P5-Asn bind at the S2 and S4 subsites, respectively. A plausible reason for this observation could be due to the fact that the peptide inhibitor used did not contain the best-fit sequence.

C. Protease in the Product-Bound Form

Beside the frame shift of the substrate-like inhibitor, the above structure failed to show a clear electron density at the C-terminal. However, the structures solved by Hsu *et al.* remedied this shortage and revealed a novel product-bound form [22]. The C-terminal residues of C145A mutant protease are intercalated into the neighboring protomer creating a product-bound structure that may resemble the intermediate during autoprocessing [22]. The two protomers of dimeric C145A, denoted "A" and "B", are oriented perpendicularly to each other, and each protomer contains three domains as those found in the wild-type structure solved previously. However, two subunits have asymmetric structures and the active site of protomer B is intercalated with the C-terminal residues 301 to 306 of protomer B' (shown with cyan ribbon) from the dimer in another asymmetric unit (Fig. (**3**)). The N-terminal residues of the protomer A (shown with green ribbon) are located near the active site of protomer B. This structure reveals the pathway in which the product is bound in the active site during the maturation process, and the six amino acids at the C-terminus of protomer B' represent the P6 to P1 sites of the autoprocessed product.

In the S1 site, the side-chain Oε1 of Gln306 (P1) forms a hydrogen bond with side chain Nε2 of His163. The side-chain Nε2 of P1-Gln donates a H-bond to the side-chain carboxylate of Glu166. Moreover, the oxygen anion at the free carboxylate end of P1-Gln forms H-bonds with the backbone NH atoms of Gly143 and Cys145. If Ala145 is replaced by Cys using computer modeling (shown in blue) to generate the active form, the Sγ atom of Cys145 is at suitable position to attack P1 carboxyl group. Residues 140–145 and 163–166 form the "outer wall" of the S1 site. The S2 site of C145A is formed by the main-chain atoms of Val186, Asp187, Arg188, and Gln189 as well as the side-chain atoms of His41, Met49, and Met165, suggesting that the P2 site prefers a bulky side chain such as Val, Leu, or Phe. The N atom in the main chain of P2-Phe interacts with the O atom of His164, and the side chain interacts with Met49, Met165, Asp187 and Arg188 through hydrophobic contacts. Residues 186–188 line the S2 subsite with some of their main-chain atoms. The side chain of P3-Thr is oriented toward bulk solvent. The O atom of the Thr accepts a H-bond (2.9 Å) from the NH of Glu166. Residues Met165, Leu167, Ser189, Thr190, and Gln192 surround the S4 subsite which also favors a hydrophobic side chain. The main-chain O atom of P4-Val accepts a H-bond (3.1 Å) from the Nε2 atom of Gln189 and the N atom of the Val donates a H-bond to the Oε1 atom of Gln189 and another main-chain NH donates a H-bond (3.3 Å) to Gln189. The side chain of P4-Val interacts with Met165 and Gln189 via hydrophobic interactions. S5 subsite is composed of the main-chain atoms of Thr190, Ala191, and Gln192. P5-Gly is not in contact with the protease. The S6 site is almost positioned at the outer area of the protein. However, the O atom and Oγ of P6-Ser still interact with the backbone N and O atoms of Gln192.

INHIBITORS OF THE SARS MAIN PROTEASE

So far, many inhibitors with low μM and sub-μM activities have been identified from high throughput random screening and rational design approaches. High throughput screening has been performed using the cell-based assay by observing the protective effect of the compounds on the VeroE6 cell infected by SARS-CoV, or the target (protease)-based assay by monitoring the inhibitory activities of the compounds on the $3CL^{pro}$ reaction. The compound banks used include FDA approved drugs, compounds with biological activities, synthetic compound libraries, known protease inhibitors, herbal medicine components, natural

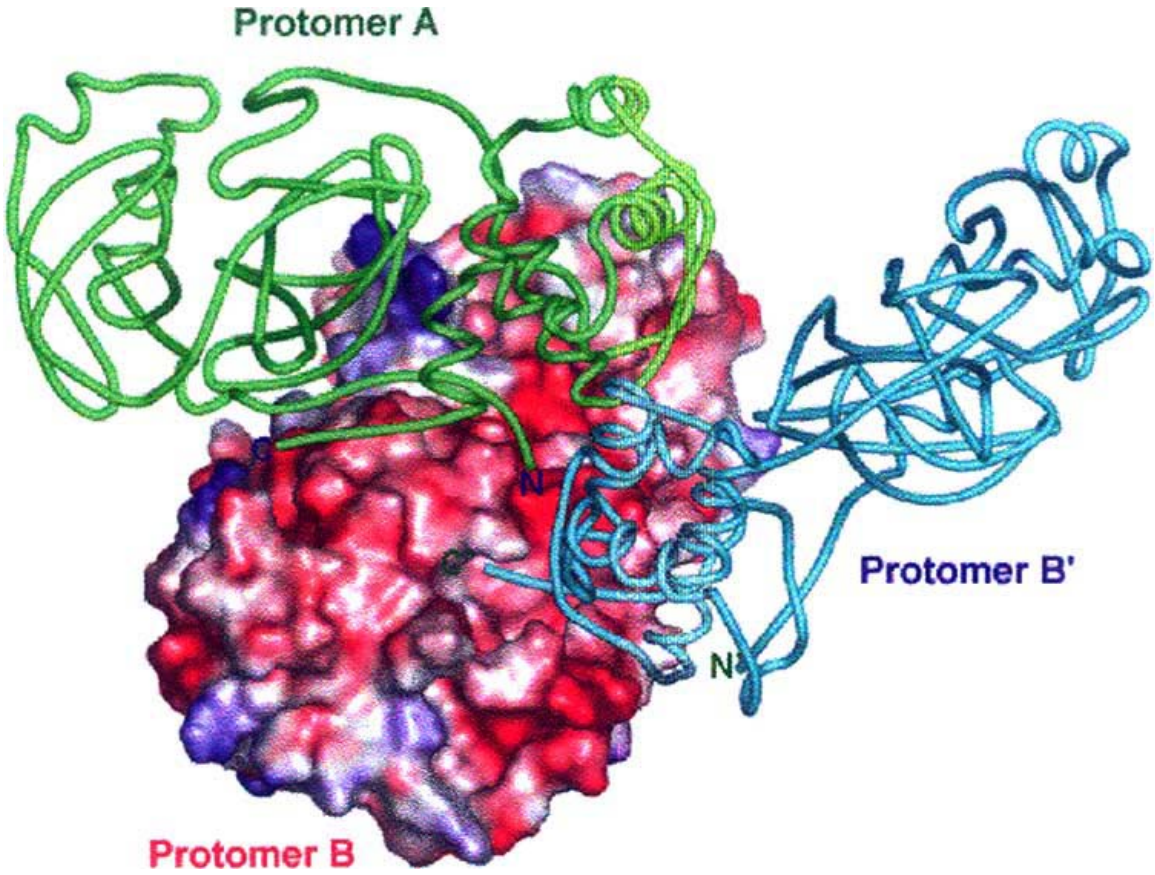

Fig. (3). A product-bound structure of SARS 3CL^{pro} resulted from the intercalation of the C-terminal six amino acids of protomer B' into protomer B, while protomer A forms a dimeric complex with protomer B. This bound protomer B' resembles the processed product.

products and others. Inhibitors from rational design approaches are those from the existing inhibitors of the human rhinovirus protease but which have been modified to fit the active site of the SARS protease, peptidomimetics designed from the substrate specificity of the protease, thiol chelating compounds targeting the active site Cys, and others as described below.

A. From High Throughput Screening

Wu *et al.* have used a Vero cell-based assay to screen many agents including about 200 drugs approved by the Food and Drug Administration, more than 8000 synthetic compounds, about 1000 traditional Chinese herbs, and almost 500 protease inhibitors. From the compounds tested, about 50 are active anti-SARS-CoV compounds, including two existing drugs Reserpine and Aescin [38]. The rationale for testing existing drugs with anti-SARS activity is because it can save time and money for developing them into anti-SARS drugs. These screenings were based on the cell cytopathogenic effect, ELSA, Western-blot analysis, immunofluorescence and flow cytometry methods. Subsequently, the fluorescence-based assay method using the Dabcyl-KTSAVLNSGFRKME-Edans substrate was performed to identify compounds that inhibit the protease. The compound that was developed as a transition-state analogue of the HIV protease (K_i = 1.5 nM toward the HIV-protease and 4 nM against feline immunodeficiency virus protease), was also identified to be active against the SARS main protease (K_i = 0.6 μM) (see TL-3 in Table **1**). Also from this study, Lopinavir (one of the two components from the anti-AIDS drug Kaletra) was showed to inhibit SARS main protease (K_i = 15 μM), which is consistent with previously observed better clinical outcome for treating SARS patients with this drug [33].

Besides Reserpine and Aescin, the existing anti-helminthic drug, niclosamide (2',5-dichloro-4'-nitrosalicylanilide), was also found to inhibit replication of SARS-CoV [46]. In Vero E6 cells, synthesis of viral spike protein and nucleocapsid protein was abolished at a niclosamide concentration of 1.6 μM as revealed by immuno-blot analysis.

Blanchard *et al.* used a FRET type (substrate = 2-aminobenzoyl-SVTLQSG-Tyr(NO_2)-R) high throughput screening approach on 50,000 drug-like small molecules to find SARS protease inhibitors [40]. Five hundred and seventy-two hits were identified from the primary screening. By a series of virtual and experimental filters, five novel small molecules (MAC-5576, MAC-8120, MAC-13985, MAC-22272, and MAC-30731) with IC_{50} = 0.5–7 μM were identified to be the SARS 3CL^{pro} inhibitors as listed in Table **1**. Their data are available for download from the McMaster HTS Lab (http://hts.mcmaster.ca/sars).

Kao *et al.* screened 50,240 structurally diverse small molecules from which they identified 104 compounds with

Table 1. SARS Main Protease Inhibitors Obtained from High Throughput Screening

Name	Structure	K_i[a] or IC_{50}[b] (μM)	Reference
TL-3	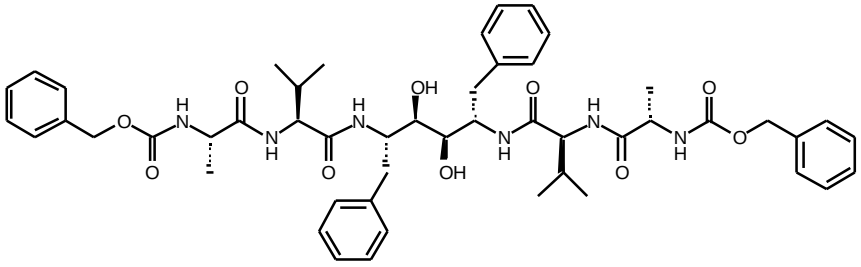	0.6[a]	38
MAC-5576	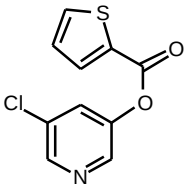	0.5[b]	40
MAC-8120	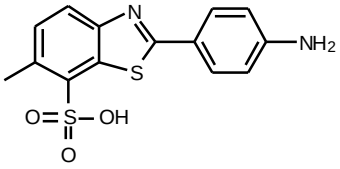	4.3[b]	40
MAC-13985	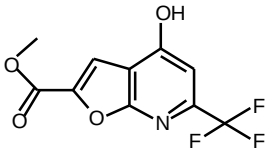	7[b]	40
MAC-22272	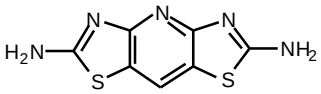	2.6[b]	40
MAC-30731	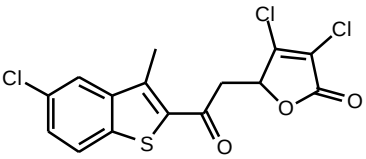	7[b]	40
MP 576	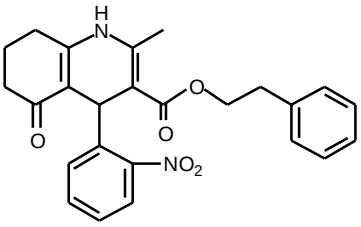	2.5[b]	47

(Table 1) Contd….

Name	Structure	K_i[a] or IC_{50}[b] (μM)	Reference
Phenylmercuric acetate	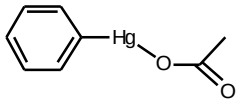	0.7[a]	48
Hexachlorophene	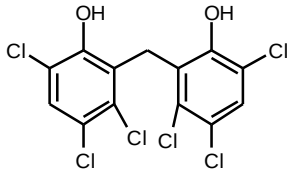	13.7[a]	48
Thimerosal	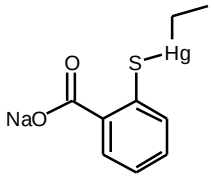	2.4[a]	48

anti-SARS–CoV activity [47]. Of these 104 compounds, 2 compounds were found to target the SARS $3CL^{pro}$ by using a HPLC-based assay method. One of the compounds (MP576 shown in Table **1**) displayed inhibitory activity with IC_{50} of 2.5 μM in the protease assay and an EC_{50} of 7 μM in the Vero cell-based SARS-CoV plaque reduction assay.

A compound library containing 960 commercially available drugs and biologically active substances was screened by Hsu *et al.* for inhibition of the SARS-CoV $3CL^{pro}$ [48]. Three hits, namely phenylmercuric acetate, thimerosal, and hexachlorophene (see Table **1** for their structures), were discovered in an *in-vitro* protease assay method. They were also effective in suppressing viral replication and the synthesis of the viral spike protein. The determination of the K_i values of phenylmercuric acetate, thimerosal, and hexachlorophene against $3CL^{pro}$ indicate that these compounds are competitive inhibitors with K_i values of 0.7 μM for phenylmercuric acetate, 2.4 μM for thimerosal, and 13.7 μM for hexachlorophene (Table **1**). Phenylmercuric acetate and thimerosal are used as pharmaceutical excipients, and are widely used as antimicrobial preservatives in parenteral and topical pharmaceutical formulations [49]. In particular, phenylmercuric acetate is used as an antimicrobial preservative in cosmetics, as a bactericide in parenterals and eye-drops, and as a spermicide. Hexachlorophene is an antibacterial agent that is a common ingredient of soaps and scrubs and is experimentally used as a cholinesterase inhibitor. The hexachlorophene derivatives were further explored as SARS protease inhibitors by Liu *et al.* [42].

Through screening from a natural product library consisting of 720 compounds, Chen *et al*. obtained two compounds, namely, tannic acid (IC_{50} = 3 μM) and 3-isotheaflavin-3-gallate (TF2B) (IC_{50} = 7 μM) as potent inhibitors of SARS $3CL^{pro}$ [50]. These two compounds belong to a group of natural polyphenols in tea, and therefore Chen *et al.* further investigated the $3CL^{pro}$ inhibitory activities of the extracts from different types of tea including green tea, oolong tea, Puer tea, and black tea. The results obtained indicated that the extracts from Puer tea and black tea were more potent in inhibiting SARS protease activity. Several known ingredients of black tea were then evaluated for anti-protease activity and theaflavin-3,3'-digallate (TF3) was found to inhibit the protease (IC_{50} <10 μM). TF3 is actually the most abundant (1.05%) theaflavin in black tea [51].

The first natural product reported to inhibit SARS-CoV replication is Glycyrrhizin although it only showed IC_{50} > 500 μM [52]. From the database of the International Species Information System, the natural compounds whose structures have 80% similarities with Glycyrrhizin, Aescin, and Reserpine were retrieved [38]. Fifteen compounds were found to be structurally related to Glycyrrhizin and Aescin, and six compounds to Reserpine. From the cell-based assay screening method, four derivatives of Glycyrrhizin and Aescin and all six analogues of Reserpine showed anti SARS-CoV activity at <100 μM. Among these compounds, Ginsenoside-Rb1 is one of the pharmacologically active components of the traditional Chinese herb, Panax ginseng [53]. However, these are not SARS protease inhibitors and their targets are not currently known.

B. From Rational Design

1. α,β-*Unsaturated Peptidomimetics*

AG7088, a ketomethyl isostere of a tripeptide-conjugated ester, is a potent inhibitor of the rhinovirus 3C protease with

an EC_{50} of 0.013 μM [54–56]. The structure of AG7088 (G = CH_2 and R = 4F-C_6H_4 as shown in Fig. (4)) incorporates a γ-lactam moiety to mimic the P1 glutamate residue and an α,β-unsaturated ester as a Michael acceptor to form a covalent linkage with the active site Cys and hence inactivate the enzyme. To improve cell membrane permeability, the P2 phenylalanine residue was replaced with a methylene isostere bearing a 4-fluorophenyl substituent. Although the model based on the crystal structure of TEGV 3C protease predicted that AG7088 can fit into the binding pocket of the SARS $3CL^{pro}$ [18], the compound is actually almost inactive towards SARS protease [22]. A series of analogues were further prepared to improve the inhibitory potencies. Shie *et al*. found that the replacement of the γ-lactam moiety with a phenylalanine side chain increased the inhibitory activity [57]. These conjugated esters were subjected to the inhibition assay using a fluorometric method [25]. As shown in Fig. (**4**), most of the tripeptide-conjugated esters (**2** and **4** series) tend to be more active than the corresponding ketomethylene isosteres (**1** and **3** series) in inhibiting the protease. For example, the compounds **3a–d** and **4a–d** with a phenyl group replacing the P1 lactam moiety showed better inhibitory activities (IC_{50} = 11–39 μM) than AG7088 (**1a**) and its analogs (**1b–d** and **2a–d**) ($IC_{50} \geq 80$ μM) [57]. From computer modeling, the P1 phenylalanine may shift to bind S2 subsite such that the α,β-unsaturated Michael acceptor is beyond the reach of the thiol moiety of Cys145 for forming a covalent linkage.

Since the best inhibitor **4d** only has an IC_{50} of 11 μM, more analogues were synthesized in microtiter plate and their inhibitory activities against SARS protease were evaluated. As shown in Table **2**, the best inhibitor (type A), an analogue of **4d**, has an IC_{50} of 1 μM. The compound also showed potent activity against SARS-CoV replication by blocking the synthesis of viral spike protein [57].

2. Anilides

With L-phenylalanine as the P1 residue, a series of peptide anilides were prepared and tested as SARS protease inhibitors [58]. Anilide **5** (Fig. (**5**)) was prepared by condensation of 2-chloro-4-nitroaniline with the acyl

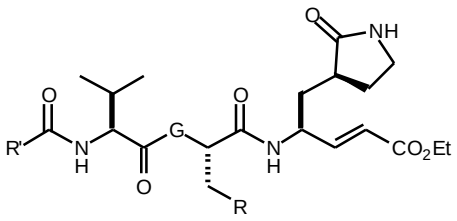

1a-d G= CH_2 **2a-d: G= NH**

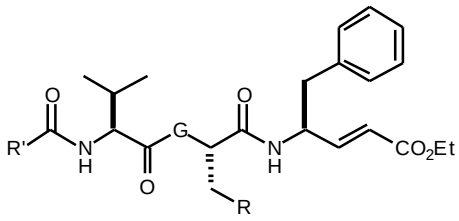

3a-d G= CH_2 **4a-d: G= NH**

a series: R = 4-F-C_6H_4, R' = 5-methyl-3-isoxazole
b series: R = 4-F-C_6H_4, R' = $PhCH_2O$
c sereis: R = Ph, R' = 5-methyl-3-isoxazole
d series: R = Ph, R' = $PhCH_2O$

Fig. (4). Compounds **1a-d** to **4a-d**.

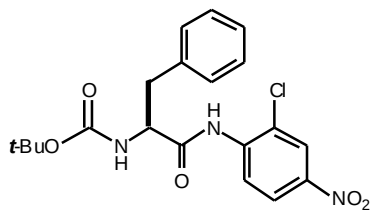

5

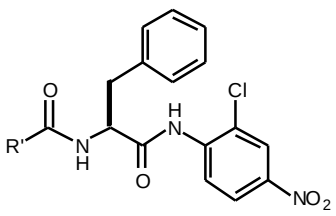

6 [60-members library]

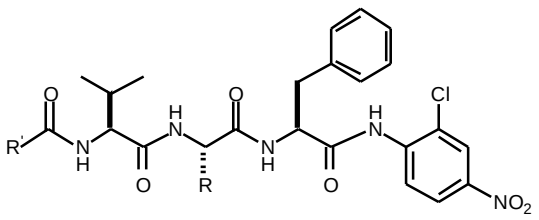

7a–x

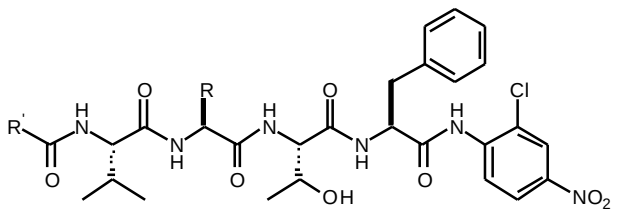

8a-x

R = ***i***-Bu, $PhCH_2$, 4-$FC_6H_4C_2$

R' = alkyl, alkoxy, aromatic, heterocyclic

Fig. (5). Compounds **5** to **8**.

Table 2. Peptidomimetics and an Isatin as SARS Main Protease Inhibitors

Inhibitor Type	Name	Structure	K_i[a] or IC_{50}[b] (μM)	Reference
A	α,β-Unsaturated ester	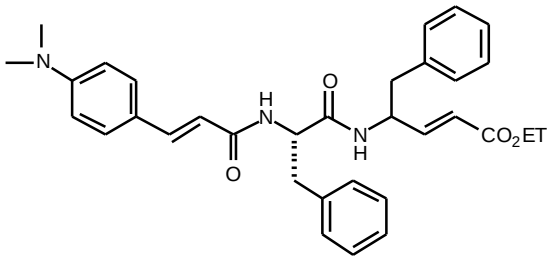	0.5[a]	57
B	Anilide	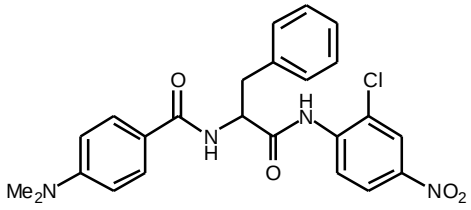	0.03[a]	58
C	Keto-glutamine analogue	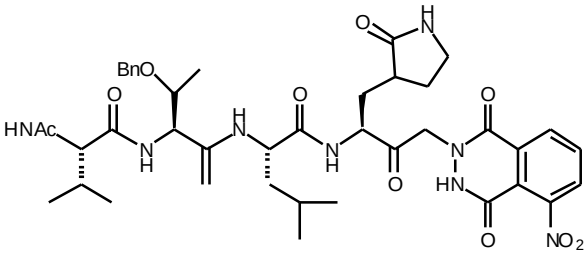	0.6[b]	61
D	Isatin	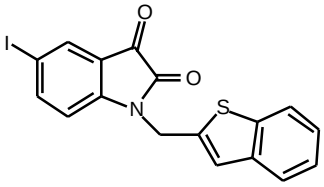	0.95[b]	63

chloride derivative of Boc-Phe-OH. Using the previously reported amide formation in a microtitre plate [59,60], the coupling reactions of a 60-member library of carboxylic acids with the amine generated by removal of the Boc group from anilide **5** afforded a 60-member library of anilide **6**. Tripeptide anilides **7a−x** (24 members) and tetrapeptide anilides **8a−x** (24 members) were also created by coupling of **5** with appropriate peptides.

Among them, an anilide compound (inhibitor type B, see Table **2**) derived from 2-chloro-4-nitroaniline, L-phenylalanine and 4-(dimethylamino)benzoic acid is the most potent inhibitor, showing a K_i of 0.030 μM. Deletion of the chloro, nitro or dimethylamino substituents from this compound significantly weakened the binding affinity. Also, replacing the dimethylamino group with a nitro group caused a reduction in inhibitor potency. According to the molecular docking, the nitro group of the compound is predicted to be hydrogen bonded with the NH of Ala46, while the chlorine atom is within 3 Å from γ-S atom of Cys145 and Nε2 atom of His41, therefore providing a possible key interaction with the catalytic dyad.

3. Keto-Glutamine Analogues

Since the SARS protease recognizes a glutamine residue at the P1 site, Jain *et al.* synthesized and evaluated a series of keto-glutamine analogues with a phthalhydrazido group at the α-position as reversible protease inhibitors [61]. Attachment of a tripeptide (Ac-Val-Thr-Leu) to these glutamine-based "warheads" (**9**) resulted in significant better inhibitors (Fig. (**6**)). N,N-Dimethylglutamine analogues (**9**) are much less potent inhibitors (10–100-fold larger IC_{50}) than cyclic glutamine analogues (**10**). The best inhibitor (inhibitor type C) is shown in Table **2**. In the modeling structures, the

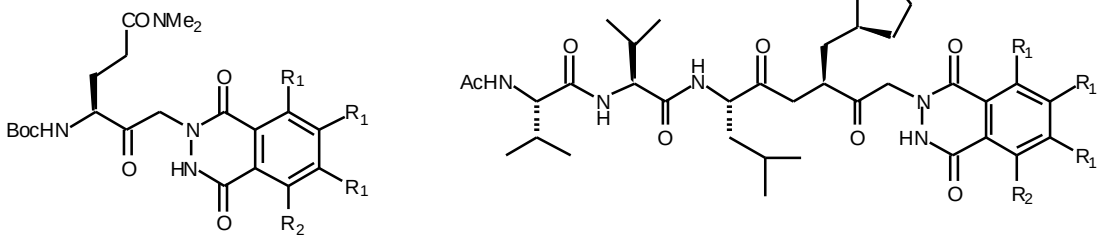

9 **10**

Fig. (6). Compounds **9** to **10**.

inhibitor is bound in an extended conformation, forming a partial β-sheet and a hydrogen bond between His163 and the P1 side chain. The modeling studies indicate that the active site of the enzyme has enough room to accommodate the bulky phthalhydrazido group. Some rearrangements of the protein, in particular residue Glu166, are required to accommodate the extra bulky group on the P1 residues.

4. Isatin

Certain isatin (2,3-dioxindole) derivatives, such as (**11**) shown in Fig. (**7**), are known potent inhibitors against the rhinovirus 3C protease [62]. This isatin core structure offers several advantages that include ease of synthesis and chemical modification. Its derivatives were tested as inhibitors for SARS $3CL^{pro}$. From a series of synthetic isatin derivatives (**12**) showing IC_{50} = 0.95–17.5 μM, the best inhibitor found is listed in Table **2** (inhibitor type D), which has an iodo or bromo in the isatin scaffold [63]. The benzothiophenemethyl side chain provides more inhibitory effect than the benzyl, heterocyclic substituted methyl, and other alkyl groups.

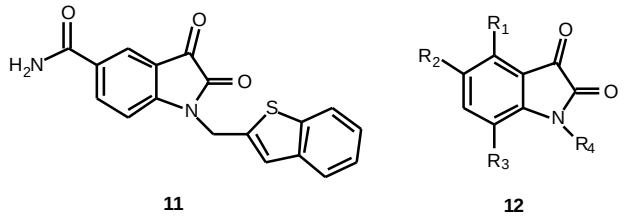

11 **12**

Fig. (7). Compounds **11** to **12**.

5. Aryl Boronic Compounds

Bacha *et al.* proposed an attractive subsite for the design of potent inhibitors, which is a cluster of Ser residues (Ser139, Ser144, and Ser147) close to the catalytic residues [35]. In fact, this Ser cluster is conserved in all known coronavirus proteases and may represent a common target of wide-spectrum coronavirus protease inhibitors. Based on the known reactivity of boronic acid compounds with the hydroxyl group in Ser residues, the inhibitory potency of bifunctional boronic acid compounds was evaluated. A chemical scafford containing two phenyl boronic groups attached to a central aromatic ring by ester linkages were tested. This compound has an inhibition constant in the low micromolar range (K_i = 4.6 μM). Different variations of the compound were prepared, including several isomers with replacement of the central aromatic ring with shorter ester linkage, and different functionalities at the phenyl boronic rings. The highest improvement in affinity was observed when the ester linkage between the aromatic rings was replaced with an amide group, thereby resulting in nanomolar inhibition constants. The structures and K_i values of the five representative inhibitors are summarized in Table **3**. The inhibitors display a mixed competitive pattern (binds to both free enzyme and enzyme-substrate complex). This may be due to the large substrate used in the kinetic measurements. These compounds inhibited the enzyme in a reversible manner.

6. Metal-Conjugated Inhibitors

As shown above in high throughput screening of 960 compounds, two compounds, phenylmercuric acetate and thimerosal, identified as potent SARS protease inhibitors contain mercury. This suggests to use metal ion as a chelator for Cys protease inhibitors since the metal ions such as Hg^{2+}, Zn^{2+}, and Cu^{2+} have high affinities for the sulfur atom of the Cys residue [64,65]. Since mercury-containing compounds may pose therapeutic hazards to a patient if orally taken, a series of zinc-containing compounds and metal ions were evaluated for SARS protease inhibition (Table **4**). The most potent inhibitor found was 1-hydroxypyridine-2-thione zinc, a competitive inhibitor with a K_i value of 0.17 μM. The involvement of the organic moiety of 1-hydroxypyridine-2-thione zinc in inhibitory activity was supported by the observations that N-ethyl-N-phenyldithiocarbamic acid zinc and toluene-3,4-dithiolato zinc showed similar K_i values (1.0 and 1.4 μM, respectively) to that of the Zn^{2+} (1.1 μM).

Zn^{2+} was previously found to be tetrahedrally coordinated by three Cys sulfurs and one His nitrogen of the 2A proteinase from a common cold virus, which is responsible for the shut-off of host-cell protein synthesis [66]. Zinc-containing compounds such as zinc acetate are added as a supplement to the drug for the treatment of Wilson's disease [67], indicating the safety of the ion for human use. Zinc salts such as zincum gluconicum (Zenullose) may be effective in treating the common cold, a disease caused by rhinoviruses, without knowledge of the molecular target [68]. Moreover, zinc ions inhibit replication of rhinoviruses [69,70]. Thus, the potential use of the zinc-conjugated compounds as a therapeutic treatment of the SARS disease rests to be explored.

Table 3. Bifunctional Aryl Boronic Compounds as SARS 3CL^{pro} Inhibitors [35]

Name	Structure	K_i (μM)
FL-078	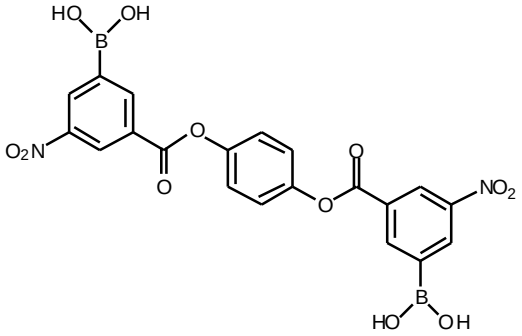	4.5
FL-101	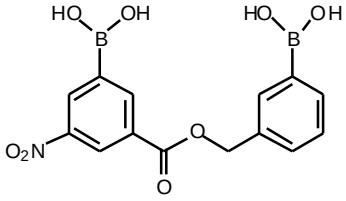	16
FL-106	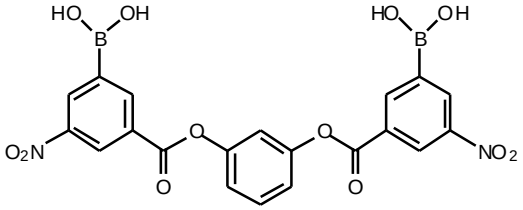	6.0
FL-136	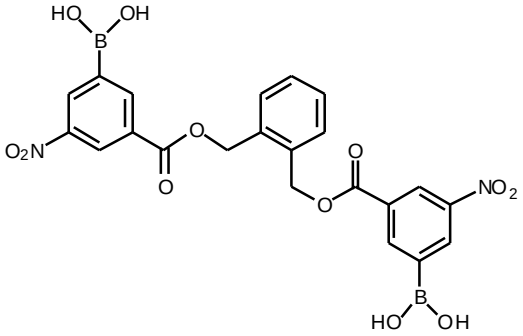	6
FL-166	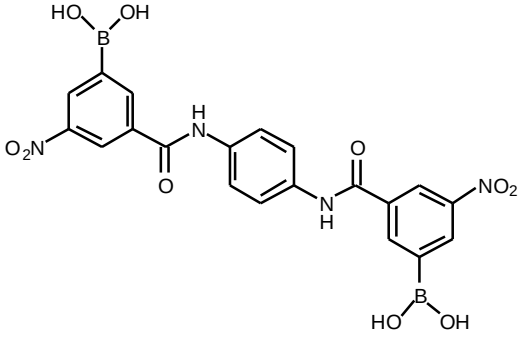	0.04

Table 4. Metal-Conjugated Compounds and Metal ions as Inhibitors of SARS 3CL^{pro} [48]

Name	Structure	K_i (μM)
Phenylmercuric nitrate	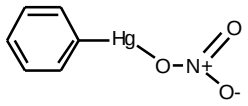	0.3
1-Hydroxypyridine-2-thione zinc	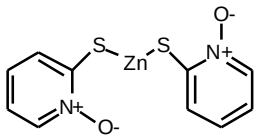	0.17
N-Ethyl-N-phenyldithio-carbamic acid zinc	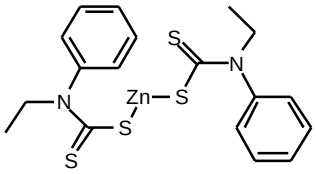	1.0
Toluene-3,4-dithiolato zinc	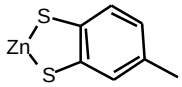	1.4
Mercuric ion	Hg^{2+}	0.5
Zinc ion	Zn^{2+}	1.1

CONCLUSION

In addition to the inhibitors identified from high throughput screening and rational design approaches, there are many other compounds that have been suggested to be potential inhibitors of SARS protease based on computer modeling [e.g., 71–78]. These compounds are not discussed here if they have not been tested in *in-vitro* assays. Some degree of structural similarity of the active site of the SARS protease with that of other 3CL proteases exist as some of the SARS protease inhibitors are derived from the previously identified inhibitors of the rhinovirus 3C protease. The newly identified compounds for SARS protease may also serve as inhibitors for other viral proteases. The rich information of the SARS protease inhibitors could provide a therapeutic solution if the SARS disease comes back in the future, and could possibly serve as new drug leads for other viral diseases. Therefore, further research in this area is clearly desirable.

ACKNOWLEDGEMENT

I thank Dr. Min-Feng Hsu and Mr. Chih-Jung Kuo to prepare some of the Figures.

ABBREVIATIONS

SARS = Severe acute respiratory syndrome

CoV = Coronavirus

TGEV = Transmissible gastroenteritis virus

HCoV = Human coronavirus

MHV = Mouse hepatitis virus

BCoV = Bovine coronavirus

PEDV = Porcine epidemic diarrhea virus

3CL^{pro} = 3C-like protease

Dabcyl = 4-(4-dimethylaminophenylazo)benzoic acid

Edans = 5-[(2-aminoethyl)amino]naphthalene-1 sulfonic acid

FRET = Fluorescence resonance energy transfer

AUC = Analytical ultracentrifugation

CMK = Chloromethylketone

REFERENCES

[1] Kuiken, T.; Fouchier, R. A.; Schutten, M.; Rimmelzwaan, G. F.; van Amerongen, G.; van Riel, D.; Laman, J. D.; de Jong, T.; van Doornum, G.; Lim, W.; Ling, A. E.; Chan, P. K.; Tam, J. S.; Zambon, M. C.; Gopal, R.; Drosten, C.; van der Werf, S.; Escriou, N.; Manuguerra, J. C.; Stohr, K.; Peiris, J. S.; Osterhaus, A. D. Newly discovered coronavirus as the primary cause of severe acute respiratory syndrome. *Lancet* **2003**, *362*, 263-270.

[2] Drosten, C.; Gunther, S.; Preiser, W.; van der Werf, S.; Brodt, H. R.; Becker, S.; Rabenau, H.; Panning, M.; Kolesnikova, L.; Fouchier, R. A.; Berger, A. Burguiere, A. M.; Cinatl, J.; Eickmann, M.; Escriou, N.; Grywna, K.; Kramme, S.; Manuguerra, J. C.; Muller, S.; Rickerts, V.; Sturmer, M.; Vieth, S.; Klenk, H. D.; Osterhaus, A. D.; Schmitz, H.; Doerr, H. W. Identification of a novel coronavirus in patients with severe acute respiratory syndrome. *N. Eng. J. Med.* **2003**, *348*, 1967-1976.

[3] Fouchier, R. A.; Kuiken, T.; Schutten, M.; van Amerongen, G.; van Doornum, G. J.; van den Hoogen, B. G.; Peiris, M.; Lim, W.; Stohr, K.; Osterhaus, A. D. Aetiology: Koch's postulates fulfilled for SARS virus. *Nature* **2003**, *423*, 240.

[4] Ksiazek, T. G.; Erdman, D.; Goldsmith, C. S.; Zaki, S. R.; Peret, T.; Emery, S.; Tong, S.; Urbani, C.; Comer, J. A.; Lim, W.; Rollin, P. E.; Dowell, S. F.; Ling, A. E.; Humphrey, C. D.; Shieh, W. J.; Guarner, J.; Paddock, C. D.; Rota, P.; Fields, B.; DeRisis, J.; Yang, J. Y.; Cox, N.; Hughes, J. M.; LeDue, J. W.; Bellini, W. J.; Anderson, L. J. A. A novel coronavirus associated with severe acute respiratory syndrome. *N. Eng. J. Med.* **2003**, *348*, 1953-1966.

[5] Peiris, J. S.; Lai, S. T.; Poon, L. L.; Guan, Y.; Yam, L. Y.; Lim, W.; Nicholls, J.; Yee, W. K.; Yan, W. W.; Cheung, M. T.; Cheng, V. C.; Chan, K. H.; Tsang, D. N.; Yung, R. W.; Ng, T. K.; Yuen, K. Y. Coronavirus as a possible cause of severe acute respiratory syndrome. *Lancet* **2003**, *361*, 1319-1325.

[6] Rota, P. A.; Oberste, M. S.; Monroe, S. S.; Nix, W. A.; Campagnoli, R.; Icenogle, J. P.; Penaranda, S.; Bankamp, B.; Maher, K.; Chen, M.-H.; Tong, S.; Tamin, A.; Lowe, L.; Frace, M.; Derisi, J. L.; Chen, Q.; Wang, D.; Erdman, D. D.; Peret, T. C. T.; Burns, C.; Ksiazek, T. G.; Rollin, P. E.; Sanchez, A.; Liffick, S.; Holloway, B.; Limor, J.; McCaustland, K.; Olsen-Rasmussen, M.; Fouchier, R.; Gunther, S.; Osterhaus, A. D. M. E.; Drosten, C.; Pallansch, M. A.; Anderson, L. J.; Bellini, W. J. Characterization of a novel coronavirus associated with severe acute respiratory syndrome. *Science* **2003**, *300*, 1394-1399.

[7] Marra, M. A.; Jones, S. J.; Astell, C. R.; Holt, R. A.; Brooks-Wilson, A.; Butterfield, Y. S.; Khattra, J.; Asano, J. K.; Barber, S. A.; Chan, S. Y.; Cloutier, A.; Coughlin, S. M.; Freeman, D.; Girn, N.; Griffith, O. L.; Leach, S. R.; Mayo, M.; McDonald, H.; Montgomery, S. B.; Pandoh, P. K.; Petrescu, A. S.; Robertson, G.; Schein, J. E.; Siddiqui, A.; Smailus, D. E.; Stott, J. M.; Yang, G. S.; Plummer, F.; Andonov, A.; Artsob, H.; Bastien, N.; Bernard, K.; Booth, T. F.; Bowness, D.; Czub, M.; Drebot, M.; Fernando, L.; Flick, R.; Garbutt, M.; Gray, M.; Grolla, A.; Jones, S.; Feldmann, H.; Meyers, A.; Kabani, A.; Li, Y.; Normand, S.; Stroher, U.; Tipples, G. A.; Tyler, S.; Vogrig, R.; Ward, D.; Watson, B.; Brunham, R. C.; Krajden, M.; Petric, M.; Skowronski, D.; Upton, C.; Roper, R. The Genome sequence of the SARS-associated coronavirus. *Science* **2003**, *300*, 1399-1404.

[8] Ruan, Y. J.; Wei, C. L.; Ee, A, L.; Vega, V. B.; Thoreau, H.; Su, S. T.; Chia, J. M.; Ng, P.; Chiu, K. P.; Lim, L.; Zhang, T.; Peng, C. K.; Lin, E. O.; Lee, N. M.; Yee, S. L.; Ng, L. F.; Chee, R. E.; Stanto, L. W.; Long, P. M.; Liu, E. T. Comparative full-length genome sequence analysis of 14 SARS coronavirus isolates and common mutations associated with putative origins of infection. *Lancet* **2003**, *361*, 1779-1785.

[9] Yeh, S. H.; Wang, H. Y.; Tsai, C. Y.; Kao, C. L.; Yang, J. Y.; Liu, H. W.; Su, I. J.; Tsai, S. F.; Chen, D. S.; Chen, P. J. The National Taiwan University SARS Research Team, Chen, D. S.; Lee, Y. T.; Teng, C. M.; Yang, P. C.; Ho, H. N.; Chen, P. J.; Chang, M. F.; Wang, J. T.; Chang, S. C.; Kao, C L.; Wang, W. K.; Hsiao, C. H.; Hsueh, P. R. Characterization of severe acute respiratory syndrome coronavirus genomes in Taiwan: molecular epidemiology and genome evolution. *Proc. Natl. Acad. Sci. USA* **2004**, *101*, 2542-2547.

[10] Snijder, E. J.; Bredenbeek, P. J.; Dobbe, J. C.; Thiel, V.; Ziebuhr, J.; Poon, L. L. M.; Guan, Y.; Rozanov, M.; Spaan, W. J. M.; Gorbalenya, A. E. Unique and conserved features of genome and proteome of SARS-coronavirus, an eraly split-off from the coronavirus group 2 lineage. *J. Mol. Biol.* **2003**, *331*, 991-1004.

[11] Thiel, V.; Ivanov, K. A.; Putics, A.; Hertzig, T.; Schelle, B.; Bayer, S.; Weissbrich, Snijder, E. J.; Rabenau, H.; Wilhelm, D.; Gorbalenya, A. E.; Ziebuhr, J. Mechanisms and enzymes involved in SARS coronavirus genome expression. *J. G. Virol.* **2003**, *84*, 2305-2315.

[12] Gao, F.; Ou, H. Y.; Chen, L. L.; Zheng, W. X.; Zhang, C. T. Prediction of proteinase cleavage sites in polyproteins of coronaviruses and its applications in analyzing SARS-CoV genomes. *FEBS Lett.* **2003**, *553*, 451-456.

[13] Allaire, M.; Chernaia, M. M.; Malcolm, B. A.; James, M. N. Picornaviral 3C cysteine proteinases have a fold similar to chymotrypsin-like serine proteinases. *Nature* **1994**, *369*, 72-76.

[14] Siddell, S. G. Ed., The Coronaviridae (Plenum, New York), **1995**.

[15] Li, W.; Moore, M. J.; Vasilieva, N.; Sui, J.; Wong, S. K.; Berne, M. A.; Somasundaran, M.; Sullivan, J. L.; Lizuriaga, K.; Greenough, T. C.; Chou, H.; Farzan, M. Angiotensin-converting enzyme 2 is a functional receptor for the SARS coronavirus. *Nature* **2003**, *426*, 450-454.

[16] Wu, H. S.; Hsieh, Y. C.; Su, I. J.; Lin, T. H.; Chiu, S. C.; Hsu, Y. F, Lin J. H.; Wang, M. C.; Chen, J. Y.; Hsiao, P. W.; Chang, G. D.; Wang, A. H.; Ting, H. W.; Chou, C. M., Huang, C. J. Early detection of antibodies against various structural proteins of the SARS-associated coronavirus in SARS patients. *J. Biomed Sci.* **2004** *11*, 117-126.

[17] Fan., K.; Wei, P.; Feng, Q.; Chen, S.; Huang, C.; Ma, L.; Lai, B.; Pei, J.; Liu, Y.; Chen, J.; Lai, L. Biosynthesis, purification, and substrate specificity of severe acute respiratory syndrome coronavirus 3C-like proteinase. *J. Biol. Chem.* **2004**, *279*, 1637-1642.

[18] Anand, K.; Ziebuhr, J.; Wadhwani, P.; Mesters, J. R.; Hilgenfeld, R. Coronavirus main proteinase (3CLpro) structure: basis for design of anti-SARS drugs. *Science* **2003**, *300*, 1763-1767.

[19] Huang, C.; Wei, P.; Fan, K.; Liu, Y.; Lai, L. 3C-like proteinase from SARS coronavirus catalyzes substrate hydrolysis by a general base mechanism. *Biochemistry* **2004**, *43*, 4568-4574.

[20] Anard, K.; Palm, G. J.; Mesters, J. R.; Siddell, S. G.; Ziebuhr, J.; Hilgenfeld, R. Structure of coronavirus main proteinase reveals combination of a chymotrypsin fold with an extra α-helical domain. *EMBO J.* **2002**, *21*, 3213-3224.

[21] Yang, H.; Yang, M.; Ding, Y.; Liu, Y.; Lou, Z.; Zhou, Z.; Sun, L.; Mo, L.; Ye, S.; Pang, H.; Gao, G. F.; Anand, K.; Bartlam, M.; Hilgenfeld, R.; Rao, Z. The crystal structures of severe acute respiratory syndrome virus main protease and its complex with an inhibitor. *Proc. Natl. Acad. Sci. USA* **2003**, *100*, 13190-13195.

[22] Hsu, M. F.; Kuo, C. J.; Chang, K. T.; Chang, H. C.; Chou, C. C.; Ko, T. P.; Shr, H. L.; Chang, G. G.; Wang, A. H.-J.; Liang, P. H. Mechanism of the maturation process of SARS-CoV 3CL protease. *J. Biol. Chem.* **2005**, *280*, 31257-31266.

[23] Shi, J. H.; Wei, Z.; Song, J. X. Dissection study on the SARS 3C-like protease reveals the critical role of the extra domain in dimerization of the enzyme: defining the extra domain as a new target of highly specific protease inhibitors. *J. Biol. Chem.* **2004**, *279*, 24765-24773.

[24] Hsu, W. C.; Chang, H. C.; Chou, C. Y.; Tsai, P. J.; Lin, P. I.. Chang, G. G. Critical assessment of important regions in the subunit association and catalytic action of the severe acute respiratory syndrome coronavirus main protease. *J. Biol. Chem.* **2005**, *280*, 22741-22748.

[25] Kuo, C. J.; Chi, Y. H.; Hsu, J. T.-A.; Liang, P. H. Characterization of SARS main protease and inhibitor assay using a fluorogenic substrate. *Biochem. Biophys. Res. Commun.* **2004**, *318*, 862-867.

[26] So, L. K.; Lau, A. C.; Yam, L. Y. Cheung, T. M.; Poon, E.; Yung, R. W.; Yuan, K. Y. Development of a standard treatment protocol for severe acute respiratory syndrome. *Lancet* **2003**, *361*, 1773-1778.

[27] Booth, C. M.; Matukas, L. M.; Tomlinson, G. A.; Rachlis, A. R.; Rose, D. B.; Dwosh, H. A.; Walmsley, S. L.; Mazzulli, T.; Avendano, M.; Derkach, P., Ephtimios, I. E.; Kitai, I.; Mederski, B. D.; Shadowitz, S. B.; Gold, W. L.; Hawryluck, L. A.; Rea, E.; Chenkin, J. S.; Cescon, D. W.; Poutanen, S. M.; Detsky, A. S. Clinical features and short-term outcomes of 144 patients with SARS in the greater Toronto area. *J. Am. Med. Assoc.* **2003**, *289*, 2801-2809.

[28] Hsu, L. Y.; Lee, C. C.; Green, J. A.; Ang, B.; Paton, N. I.; Lee, L.; Villacian, J. S.; Lim, P. L.; Earnest, A.; Leo, Y. S. Severe acute respiratory syndrome (SARS) in Singapore: clinical features of index patient and initial contacts. *Emerg. Infect. Dis.* **2003**, *9*, 713-717.

[29] Zhong, N. S.; Zeng, G. Q. Our stratgies for fighting severe acute respiratory syndrome (SARS). *Am. J. Respir. Care Med.* **2003**, *168*, 7-9.

[30] Ho, W. Hong Kong Hospital Authority Working Group on SARS, Central Committee of Infection Control. Guideline on management of severe acute respiratory syndrome (SARS). *Lancet* **2003**, *361*, 1313-1315.

[31] Cinatl, J.; Morgenstern, B.; Bauer, G.; Chandra, P.; Rabenau, H.; Doerr, H. W. Treatment of SARS with human interferons. *Lancet* **2003**, *362*, 293-294.

[32] Tsang, K.; Seto, W. H. Severe acute respiratory syndrome: scientific and anecdotal evidence for drug treatment. *Curr. Opin. Invest. Drugs* **2004**, *5*, 179-185.

[33] Chan, K. S.; Lai, S. T.; Chu, C. M.; Tsui, E.; Tam, C. Y.; Wong, M. M.; Tse, M. W.; Oue, T. L.; Peiris, J. S.; Sung, J.; Wong, V. C.; Yuan, K. Y. Treatment of severe acute respiratory syndrome with lopinavir/ritonavir: a multicentre retrospective matched cohort study. *Hong Kong Med. J.* **2003**, *9*, 399-406.

[34] Tan, E. L.; Ooi, E. E.; Lin, C. Y.; Tan, H. C.; Ling, A. E.; Lim, B.; Stanton, L. W. Inhibition of SARS coronavirus infection *in vitro* with clinically approved antiviral drugs. *Emerg. Infect. Dis.* **2004**, *10*, 581-586.

[35] Bacha, U.; Barrila, J.; Velazquez-Campoy, A.; Leavitt, S. A.; Freire, E. Identification of novel inhibitors of the SARS coronavirus main protease $3CL^{pro}$. *Biochemistry* **2004**, *43*, 4906-4912.

[36] Sun, H.; Luo, H.; Yu, C.; Sun, T.; Chen, J.; Peng, S.; Qin, J.; Shen, J.; Yang, Y.; Xie, Y.; Chen, K.; Wang, Y.; Shen, X.; Jiang, H. Molecular cloning, expression, purification, and mass spectrometric characterization of 3C-like protease of SARS coronavirus. *Prot. Expr. Puri.* **2004**, *32*, 302-308.

[37] Fan, K.; Ma, L.; Han, X.; Liang, H.; Wei, P.; Liu, Y.; Lai, L. The substrate specificity of SARS coronavirus 3C-like proteinase. *Biochem. Biophys. Res. Commun.* **2005**, *329*, 934-940.

[38] Wu, C. Y.; Jan, J. T.; Ma, S. H.; Kuo, C. J.; Juan, H. F.; Cheng, Y. S.; Hsu, H. H.; Huang, H. C.; Wu, D.; Brik, A.; Liang, F. S.; Liu, R. S.; Fang, J. M.; Chen, S. T.; Liang, P. H.; Wong, C. H. Small moleculaes targeting severe acute respiratory syndrome human coronavirus. *Proc. Natl. Acad. Sci. USA.* **2004**, *101*, 10012-10017.

[39] Matayoshi, E. D.; Wang, G. T.; Krafft, G. A.; Erickson, J. Novel fluorogenic substrates for assaying retroviral proteases by resonance energy transfer. *Science* **1990**, *247*, 954-958.

[40] Blanchard, J. E.; Elowe, N. H.; Huitema, C.; Fortin, P. D.; Cechetto, J. D.; Eltis, L. D.; Brown, E. D. High-throughput screening identifies inhibtors of the SARS coronavirus main protease. *Chem. Biol.* **2004**, *11*, 1445-1453.

[41] Liu, Y. C.; Huang, V.; Chao, T. C.; Hsiao, C. D.; Lin, A.; Chang, M. F.; Chow, L. P. Screening of drugs by FRET analysis identifies inhibitors of SARS-CoV 3CL protease. *Biochem. Biophys. Res. Commun.* **2005**, *333*, 194-199.

[42] Batra, R.; Khayat, R.; Tong, L. Molecular mechanism for dimerization to regulate the catalytic activity of human cytomegalovirus protease. *Nat. Struct. Biol.* **2001**, *8*, 810-817.

[43] Zhang, Z. Y.; Poorman, R. A.; Maggiora, L. L.; Heinrikson, R. L.; Kezdy, F. J. Dissociative inhibition of dimeric enzymes. Kinetic characterization of the inhibition of HIV-1 protease by its COOH-terminal tetrapeptide. *J. Biol. Chem.* **1991**, *266*, 15591-15594.

[44] Chien, C. H.; Huang, L. H.; Chou, C. Y.; Chen, Y. S.; Han, Y. S.; Chang, G. G.; Liang, P. H.; Chen, X. (2004) One site mutation disrupts dimer formation in human DPP-IV proteins. *J. Biol. Chem.* **2004**, *279*, 52338-52345.

[45] Chou, C. Y.; Chang, H. C.; Hsu, W. C.; Lin, T. Z.; Lin, C. H.; Chang, G. G. Quaternary structure of the severe acute respiratory syndrome (SARS) coronavirus main protease. *Biochemistry* **2004**, *43*, 14958-14970.

[46] Wu, C. J.; Jan, J. T.; Chen, C. M.; Hsieh, H. P.; Hwang, D. R.; Liu, H. W.; Liu, C. Y.; Huang, H. W.; Chen, S. C.; Hong, C. F.; Lin, R. K.; Chao, Y. S.; Hsu, J. T.-A.. Inhibition of severe acute respiratory syndrome coronavirus replication by niclosamide. *Antimicrob. Agents Chemother.* **2004**, *48*, 2693-2696.

[47] Kao, R. Y.; Tsui, W. H. W.; Lee, T. S. W.; Tanner, J. A.; Watt, R. M.; Huamg, J. D.; Hu, L.; Chen, G.; Chen, Z.; Zhang, L.; He, T.; Chan, K. H.; Tse, H.; To, A. P. C.; Ng, L. W. Y.; Wong, B. C. W.; Tsoi, H. W.; Yang, D.; Ho, D. D.; Yuen, K. Y. Identification of novel small-molecule inhibitors of severe acute respiratory syndrome-associated coronavirus by chemical genetics. *Chem. Biol.* **2004**, *11*, 1293-1299.

[48] Hsu, J. T. A.; Kuo, C. J.; Hsieh, H. P.; Wang, Y. C.; Huang, K. K.; Lin, C. P.; Huang, P. F.; Chen, X.; Liang, P. H. Evaluation of metal-conjugated compounds as inhibitors of 3CL protease of SARS-CoV. *FEBS Lett.* **2004**, *574*, 116-120.

[49] Rowe, R. C.; Sheskey, P. J.; Weller, P. J. Handook of Pharmaceutical Excipients, 4th Ed., Pharmaceutical Press, **2003**.

[50] Chen, C. N.; Lin, C. P.C.; Huang, K. K.; Chen, W. C.; Hsieh, H. P.; Liang, P. H.; Hsu, J. T.A. Inhibition of SARS-CoV 3C-like protease activity by Theaflavin-3,3-digallate (TF3). *eCAM* **2005**, *2*, 209-215.

[51] Leung, L. K.; Su, Y.; Chen, R.; Zhang, Z.; Huang, Y.; Chen, Z. Y. Theaflavins in black tea and catechins in green tea are equally effective antooxidants. *J. Nutr.* **2001,** *131*, 2248-2251.

[52] Cinatl, J.; Morgenstern, B.; Bauer, G.; Chandra, G.; Rabenau, H.; Doerr, H. W. Glycyrrhizin, an active component of liquorice roots, and replication of SARS-associated coronavirus. *Lancet* **2003**, *361*, 2045-2046.

[53] Jeong, C. S.; Hyun, J. E.; Kim, Y. S. Ginsenoside Rb1: the anti-ulcer constituent from the head of Panax ginseng. *Arch. Pharmacal. Res.* **2003**, *26*, 906-911.

[54] Dragovich, P. S.; Prins, T. J.; Zhou, R.; Webber, S. E.; Marakovits, J. T.; Fuhrman, S. A.; Patick, A. K.; Matthews, D. A.; Lee, C. A.; Ford, C. E.; Burke, B. J.; Rejto, P. A.; Hendrickson, T. F.; Tuntland, T.; Brown, E. L.; Meador, J. W., III; Ferre, R. A.; Harr, J. E. V.; Kosa, M. B.; Worland, S. T. Structure-based design, synthesis, and biological evaluation of irreversible human rhinovirus 3C protease inhibitors. 8. Pharmacological optimization of orally bioavailable 2-pyridone-containing peptidomimetics. *J. Med. Chem.* **1999**, *42*, 1213−1224.

[55] Patick, A. K.; Binford, S. L.; Brothers, M. A.; Jackson, R. L.; Ford, C. E.; Diem, M. D.; Maldonado, F.; Dragovich, P. S.; Zhou, R.; Prins, T. J.; Fuhrman, S. A.; Meador, J. W.; Zalman, L. S.; Matthews, D. A.; Worland, S. T. *In vitro* antiviral activity of AG7088, a potent inhibitor of human rhinovirus 3C protease. *Antimicrob. Agents Chemother.* **1999**, *43*, 2444−2450.

[56] Matthews, D. A.; Dragovich, P. S.; Webber, S. E.; Fuhrman, S. A.; Patick, A. K.; Zalman, L. S.; Hendrickson, T. F.; Love, R. A.; Prins, T. J.; Marakovits, J. T.; Zhou, R.; Tikhe, J.; Ford, C. E.; Meador, J. W.; Ferre, R. A.; Brown, E. L.; Binford, S. L.; Brothers, M. A.; Delisle, D. M.; Worland, S. T. Structure-assisted design of mechanism-based irreversible inhibitors of human rhinovirus 3C protease with potent antiviral activity against multiple rhinovirus serotypes. *Proc. Natl. Acad. Sci. USA* **1999**, *96*, 11000−11007.

[57] Shie, J. J.; Fang, J. M.; Kuo, T. H.; Kuo, C. J.; Liang, P. H.; Huang, H. J.; Wu, Y. T.; Jan, J. T.; Cheng, Y. S.; Wong, C. H. Inhibition of the severe acute respiratory syndrome 3CL protease by peptidomimetic alpha,beta-unsaturated esters. *Bioorg. Med. Chem.* **2005**, *13*, 5240-5252.

[58] Shie, J. J.; Fang, J. M.; Kuo, C. J.; Kuo, T. H.; Liang, P. H.; Huang, H. J.; Yang, W. B.; Lin, C. H.; Chen, J. L.; Wu, Y. T.; and Wong, C. H. Discovery of potent anilide inhibitors against the severe acute respiratory syndrome 3CL protease. *J. Med. Chem.* **2005**, *48*, 4469-4473.

[59] Wu, C. Y.; Chang, C. F.; Chen, J. S.-Y.; Wong, C. H.; Lin, C. H. Rapid diversity-oriented synthesis in microtiter plates for in-situ screening: discovery of potent and selective α-fucosidase inhibitors. *Angew. Chem. Int. Ed.* **2003**, *42*, 4661-4664.

[60] Chang, C. F.; Ho, C. W.; Wu, C. Y.; Chao, T. A.; Wong, C. H.; Lin, C. H. Discovery of picomolar slow tight-binding inhibitors of α-fucosidase. *Chem. Biol.* **2004**, *11*, 1301-1306.

[61] Jain, R. P.; Pettersson, H. I.; Zhang, J.; Aull, K. D.; Fortin, P. D.; Huitema, C.; Eltis, L. D.; Parrish, J. D.; James, M. N. G.; Wishart, D. S.; and Vederas, J. C. Syntehsis and evaluation of keto-glutamine analogues as potent inhibitors of severe acute respiratory syndrome 3CLpro. *J. Med. Chem.* **2004**, *47*, 6113-6116.

[62] Webber, S. E.; Tikhe, J.; Worland, S. T.; Fuhrman, S. A.; Hendrickson, T. F.; Matthews, D. A.; Love, R. A.; Patrick, A. K.; Meador, J. W.; Ferre, R. A.; Brown, E. L.; DeLisle, D. M.; Ford, C. E.; Binford, S. L. Design, synthesis, and evaluation of nonpeptidic inhibitors of human rhinovirus 3C protease. *J. Med. Chem.* **1996**, *39*, 5072-5082.

[63] Chen L. P.; Wang, Y. C.; Lin, Y. W.; Chou, S. Y.; Chen, S. F.; Liu, L. T.; Wu, Y. T.; Kuo, C. J.; Chen, T. S. S.; Juang, S. H. Synthesis and evaluation of isatin derivatives as effective SARS coronavirus 3CL protease inhibitors. *Bioorg. Med. Chem. Lett.* **2005**, *15*, 3058-3062.

[64] Lockwood, T. D. Cys-His proteases are among the wired proteins of the cell. *Arch. Biochem. Biophys.* **2004**, *432*, 12-24.

[65] Liu, X.; Liang, J.; Ghazi, A. M.; Frey, T. K. Characterization of the zinc binding activity of the rubella virus nonstructural protease. *J. Virol.* **2000**, *74*, 5949-5956.

[66] Petersen, J. F.; Cherney, M. M.; Liebig, H. D.; Skern, T.; Kuechler, E.; James, M. N. The structure of the 2A proteinase from a common cold virus: a proteinase responsible for the shut-off of host-cell protein synthesis. *EMBO J.* **1999**, *18*, 5463-5475.

[67] Brewer, G. J.; Johnson, V. D.; Dick, R. D.; Hedera, P.; Fink, J. K. and Kluin, K. J. Treatment of Wilson's disease with zinc. XVII: treatment during pregnancy. *Hepatology* **2000**, *31*, 364-370.

[68] Mossad, S. B. Effect of zincum gluconicum nasal gel on the duration and symptom severity of the common cold in otherwise healthy adults. *Q. J. Med.* **2003**, *96*, 35-43.

[69] Korant, B. D.; Kauer, J. C.; Butterworth, B. E. Zinc ions inhibit replication of rhinoviruses. *Nature* **1974**, *248*, 588-590.

[70] Merluzzi, V. J., Cipriano, D., McNeil, D., Fuchs, V., Supeau, C., Rosenthal, A. S., and Skiles, J. W. Evaluation of zinc complexes on the replication of rhinovirus 2 *in vitro*. *Res. Commun. Chem. Pathol. Pharmacol.* **1989**, *66*, 425-440.

[71] Jenwitheesuk, E.; Samudrala, R. Identifying inhibitors of the SARS coronavirus proteinase. *Bioorg. Med. Chem. Lett.* **2003**, *13*, 3989-3992.

[72] Chou, K. C.; Wei, D. Q.; Zhong, W. Z. Binding mechanism of coronavirus main proteinase with ligands and its implication to drug design against SARS. *Biochem. Biophys. Res. Commun.* **2003**, *308*, 148-151.

[73] Xiong, B.; Gui, C. S.; Xu, X. Y.; Luo, C.; Chen, J.; Luo, H. B.; Chen, L. L.; Li, G. W.; Sun, T.; Yu, C. Y.; Yue, L. D.; Duan, W. H.; Shen, J. K.; Qin, L.; Li, Y. X.; Chen, K. X.; Luo, X. M.; Shen, X.; Shen, J. H.; Jiang, H. L. A 3D model of SARS-CoV 3CL proteinase and its inhibitors design by virtual screening. *Acta. Pharmacol. Sin.* **2003**, *24*, 497-504.

[74] Zhang, X. W.; Yap, Y. L. Old drug as lead compounds for a new disease? Binding analysis of SARS coronavirus main protease with HIV, psychotic and parasite drugs. *Bioorgan. Med. Chem.* **2004**, *12*, 2517-2521.

[75] Toney, J. H.; Navas-Martin, S.; Weiss, S. R.; Koeller, A. Sabadinine: A potential non-peptide anti-Severe Acute Respiratory Syndrome agent identified using structure-aided design. *J. Med. Chem.* **2004**, *47*, 1079-1080.

[76] Rajnarayanan, R. V.; Dakshanamurthy, S.; Pattabiraman, N. Teaching old drugs to kill new bugs: structure-based discovery of anti-SARS drugs. *Biochem. Biophys, Res. Commun.* **2004**, *321*, 370-378.

[77] Zhang, X. W.; Yap, Y. L.; Altmeyer, R. M. Generation of predictive pharmacophore model for SARS-coronavirus main proteinase. *Eur. J. Med. Chem.* **2005**, *40*, 57-62.

[78] Du, Q.; Wang, S.; Wei, D.; Sirois, S.; Chou, K. C. Molecular modeling and chemical modification for finding peptide inhibitor against severe acute respiratory syndrome coronavirus main proteinase. *Anal. Biochem.* **2005**, *337*, 262-270.